water

MDPI

Article

Sloshing Motion in a Real-Scale Water Storage Tank under Nonlinear Ground Motion

Heng Jin [1,2], Ruiyin Song [1,*] and Yi Liu [1,3]

1 Ningbo Institute of Technology, Zhejiang University, Ningbo 315000, China; jinheng@nit.zju.edu.cn (H.J.); liuyilulu@nit.zju.edu.cn (Y.L.)
2 Ningbo Institute of Dalian University of Technology, Ningbo 315016, China
3 Ningbo Shenglong Group Company Limited, Ningbo 315105, China
* Correspondence: sry@nit.zju.edu.cn

Received: 9 June 2020; Accepted: 18 July 2020; Published: 24 July 2020

check for updates

Abstract: Water storage tanks in cities are usually large and are occasionally affected by earthquakes. A sudden earthquake can cause pressure pulses that damage water containers severely. In this study, the sloshing motion in a high filling level tank caused by seismic excitation is investigated by the numerical method in a 2D model. Two well-studied strong earthquakes are used to analyze the broadband frequency nonlinear displacement of the tank both in the longitudinal and vertical directions. Based on careful experimental verification, the free surface motion and the elevations at the side wall are captured, and the sloshing pressure response is examined. The results show that the 2D section of the cylindrical tank can be used to estimate the maximum response of the 3D sloshing, and the water motions under the seismic excitations are consistent with the modal characteristics of the sloshing. The time histories response of the water motion reflected that the sloshing response is hysteretic compared with the seismic excitation. The anti-seismic ability of the damping baffle shows that its effect on sloshing pressure suppression is limited, and further study on the seismic design of water tanks in earthquake-prone regions is needed.

Keywords: sloshing; ground motion; water storage tank; damping baffle; response analysis

1. Introduction

Water is the source of life. It is an essential element in human production and life. Almost all fields including agricultural irrigation, hydropower, climate, etc., are inextricably linked to water; therefore, the management of the water resources is necessary. The utilization, environmental health, and storage safety of the water resources all are part of the management of water. The water tanks, as the container for water storage, are usually large and have higher safety standards. Therefore, it is very important to ensure the safety of the water tank under external environmental loads such as an earthquakes or wind.

In high seismic regions, the seismic design of water tanks has attracted more attention from structural engineers as the urban water storage demand increases [1,2]. The design of a liquid container is of particular concern when the sloshing frequency is close to the seismic excitation frequency (i.e., resonance), because pressure pulses from the dynamic load may seriously damage the system [3,4]. Sloshing has been widely studied as a typical fluid motion phenomenon [5]. The free surface motion and the resonance frequency location are the key factors determining the hydrodynamic load in the container, and the movement of the water body in the tank is closely related to external excitations. Therefore, a more careful evaluation of the hydrodynamics performance of a sloshing water storage tank under external excitation is required.

At first, researchers focused on the sloshing phenomena subject to a harmonic excitation [6–9]. As was shown, sloshing characteristics were influenced by tank parameters such as water depth [10], tank shape [7,11,12], baffle type [9,11,13–15], external excitation [6], and so on [16]. A series of analytical [15,17], numerical [10,18], and experimental [19,20] methods were established for solving the sloshing problem under different conditions. However, Chen et al. [21] compared the response of liquid tanks under harmonic excitations with those under the ground motion excitation, and they found that simple harmonic excitation cannot replace nonlinear seismic excitation for the seismic analysis of liquid tanks, because seismic excitation usually consists of a broadband frequency vibration, and harmonic excitation only contains a single frequency. The primary frequencies of the ground motion decrease with the increasing intensity of a seismic event. The frequencies of a strong earthquake are usually distributed across a lower range, which is similar to the natural frequencies of many large industrial tanks [22]. Therefore, the sloshing phenomena under various types of seismic excitation may differ.

In order to improve the computational efficiency and reduce the costs, a small-scale geometric model was usually used on a tank whose characteristic length in the excitation direction was between 0.6 and 1 m [23,24]. However, the ground motion has not been proportionally scaled, along with an overestimated sloshing response estimated. Meanwhile, the filling levels of the tank in the previous study were usually selected to be at a shallow depth [25–27] (depth/tank's length < 0.1) or near critical depth (depth/tank length ≈ 0.337) [25,28] to study the nonlinear sloshing phenomenon. The limited cases considering high filling level conditions focused on the problem of the impact of water on the tank roof under the large displacement [29]. Jin et al. [19] tested the sloshing response in a high filling level tank with filling depth(d)/tank length(L) = 0.5 by the experiments, and they found that the water motion tended to be linear in such a deep tank, which differed from the violent nonlinear sloshing in the shallow water tank. For city water storage tanks, the size is large, and the filling level is high. The load from the sudden ground movement will be the main threat to its safety. Unlike the long-term loads such as wind or waves in tuned liquid damper systems on high-rise buildings or the liquid tanks in ships, the seismic wave is a non-periodic impulse vibration with a broadband frequency characteristic. Under this condition, the motion response of the water in the container may differ from the previous studies.

In this research, the liquid sloshing motion in a real-scale water storage tank was investigated under several selected ground motions, using the computational fluid dynamic (CFD) software—OpenFOAM® (Version: 1906, OpenCFD, Bracknell, UK) [30]. The high filling level, real-scale tank, and ground motion were used to distinguish the present water motion from previous sloshing studies in other fields. First, the numerical model and the governing equation were introduced. The problem of seismic response of the water tank was described in detail. Then, the numerical model was used to discuss the motion of the free surface in the water tank and the sloshing control effect by the damping plate after rigorous numerical verification.

2. Numerical Method and Model

2.1. Governing Equation

Navier–Stokes equations [30] were used to describe the incompressible, viscous, water flows in the present numerical model. In the sloshing problem, the sloshing flow was usually assumed to be a laminar flow, and it can give an acceptable result when the free surface motion was small [10,16,31]. In this study, the laminar model was used to solve the governing equations below:

$$\frac{\partial u_i}{\partial x_i} = 0 \tag{1}$$

$$\frac{\partial u_i}{\partial t} + u_{\mathrm{i}} \frac{\partial u_i}{\partial x_j} = -\frac{1}{\rho}\frac{\partial p}{\partial x_i} + \frac{\mu}{\rho}\frac{\partial}{\partial x_j}\frac{\partial u_i}{\partial x_j} + f_{\mathrm{body}} \tag{2}$$

The meaning of the variables in the above equation is as follows: ρ is the density of the water, u_i represents the velocity components in the i direction, x_i ($i = x$, y in two-dimensions and x, y, z in three-dimensions), p is the pressure, μ is the dynamic viscosity, and f_{body} represents the body forces, such as gravity. The Finite Volume Method (FVM) was used for spatial discretization of the partial differential equations. The quantities of interest, e.g., the pressure and velocity of fluid, were stored at the centroid of control volumes. The volume-of-fluid (VoF) method was selected to capture the free surface. The volume fraction of the fluid was defined in the transport equation:

$$\rho = \alpha_{\text{water}}\rho_{\text{water}} + (1 - \alpha_{\text{water}})\rho_{\text{air}},\ v = \alpha_{\text{water}}v_{\text{water}} + (1 - \alpha_{\text{water}})v_{\text{air}}, \tag{3}$$

where α_{water} is the volume fraction of water and v is the kinematic viscosity. The volume fraction of water was expressed by the following equation:

$$\frac{\partial \alpha}{\partial t} + \alpha\frac{\partial u_i}{\partial x_i} = 0 \tag{4}$$

The variable α represents water when its value is equal to 1 and the interface of water and air when $\alpha \approx 0.5$.

2.2. Numerical Model

The sloshing model was established based on OpenFOAM (Version: 1906), and the results were solved through the interFoam solver. The solution process of the new interFoam solver is shown in Figure 1. The PIMPLE algorithm, a combination of PISO (Pressure Implicit with Splitting of Operator) and SIMPLE (Semi-Implicit Method for Pressure-Linked Equations), in Figure 1 was applied to solve the pressure–velocity coupling relationship. More detail of the solver, the boundary conditions, and other setups can refer to the previous study [18]. The mesh near the free surface was refined to improve the accuracy of free surface capture. The 6 degree-of-freedom (6DoF) tank movements were imposed through a formatted displacement of time series data.

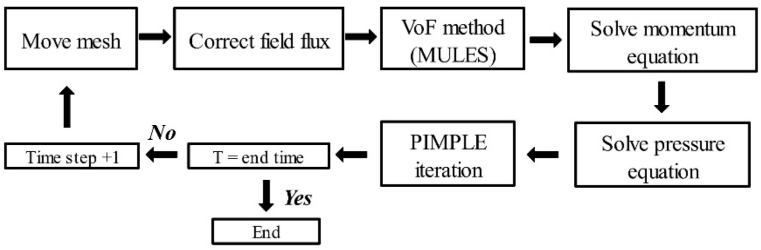

Figure 1. Solution process of the interFoam solver.

2.3. Problem Description

To investigate the water motion in a real-scale tank, which was subjected to the ground motions, the present numerical model was validated first with experimental tests. The experimental water tank was 1 m (L) × 0.8 m (H) × 0.1 m (B) as shown in Figure 2, and the filling depth d/L was 0.5. The amplitude of horizontal displacement A/L was 0.0025, and the excitation frequency ω/ω_1 = 0.996 in Figure 2b and ω/ω_1 = 0.603 in Figure 2c (ω_1 is the first-order natural frequency of the liquid tank). The detailed experimental setup and the arrangement of the experimental system were the same as the author's previous experimental device, and there is no baffle installation in the validation test [19]. Then, the free surface shape and the flow motion were compared carefully in Figure 2b,c. The heights of the free surface curves and the time history of the free surface elevation along the left tank wall are also shown in Figure 3 and validated based on the experimental result and theory model [32]. The uncertainty analysis was conducted to obtain the standard error and confidence level of the experimental result. The numerical result fell within the 95% confidence interval. The theoretical results were a bit biased after 14 s, which may be because it did not consider the viscosity and compressibility of the fluid. In general, the error of the experimental tests was acceptable, and the result of the numerical model was credible. Furthermore, the ability of the present model to simulate strong nonlinear water motion was also verified with the experimental test of Faltinsen et al. [33] in Figure 4. The tank's internal dimensions were 1.0 m × 0.98 m × 0.1 m (length × height × breadth), the d/L was 0.4, and the A/L was 0.01. The good agreements were obtained in two sets of tests. The present numerical using a laminar assumption can be used to analyze the sloshing problem.

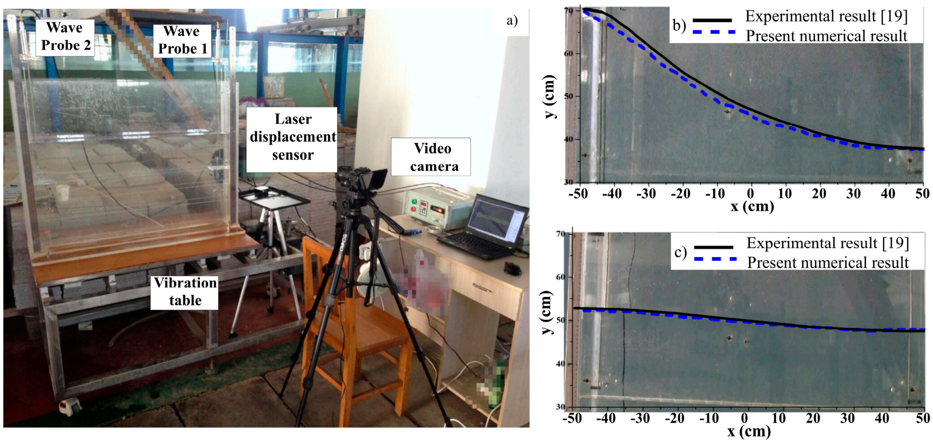

Figure 2. Free surface shape of sloshing water in a rectangular tank under horizontal harmonic excitation, (**a**) data acquisition system, (**b**) Resonant sloshing, $\omega/\omega_1 = 0.996$, (**c**) non-resonant sloshing, $\omega/\omega_1 = 0.603$.

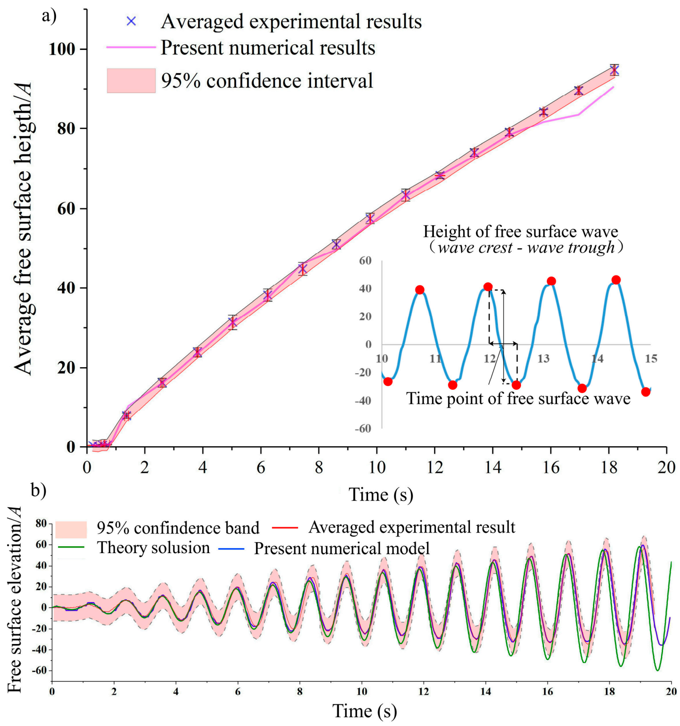

Figure 3. The validation of the present numerical model with experimental tests [19] and theoretical solution [32], $\omega/\omega_1 = 0.996$, $A/L = 0.0025$, $d/L = 0.5$. (**a**) Uncertainty analysis of three experimental tests, the error bars indicated a Standard Error of time (X-error) and height (Y-error) of the free surface wave. (**b**) Red shallow area represented the prediction limit of the average experimental result at a 95% confidence level.

Figure 4. Flow motion through the vertical slot baffle in Faltinsen's experimental tests [33], τ is the porosity of the baffle, (**a**) τ = 0.085, ω/ω_1 = 1.328, Time = 14 s, (**b**) τ = 0.527, ω/ω_1 = 0.96, Time = 46 s.

Then, a real-scale water tank in Haroun [34] was selected as the baseline structure for this study. This tank was located in Los Angeles, which is a city with potential earthquakes risk [35]. The tank geometry is shown in Figure 5, with 18 m (*Diameter* (*D*)) × 18.25 m (*Height*′(*H*′)). The filling depth *d* was 10.8 m (60% *D*), and then the tank can be regarded as a slender [36] or deep water tank ($2d/D > 1$). This filling level was larger than the value of $d/D = 0.4$, and therefore, the wave motion resembles a standing wave with the largest free surface elevations at the tank walls [37]. The Froude number is the only dimensionless number to be considered if there is a scaled model used. In CFD analysis, simplified assumptions and models are usually required to make the calculation process economically viable. Therefore, a two-dimensional (2D) *Oxy* section of the cylindrical tank was extracted to build a numerical water tank. The size of the numerical tank was the same as the real water tank in *X* and *Y* directions. The Z direction in the numerical model was a symmetry plane. The mesh dependence was tested to ensure that the present mesh size can capture the sloshing surface well in Table 1. Finally, the medium mesh size with Δx = 0.15 m, Δy = 0.05 m was selected, and the mesh near the free water surface was refined locally. Two well-studied ground motions, the 1940 Imperial Valley (IV) and 1971 San Fernando (SF) earthquakes [38], were selected for the following analysis. They transferred a nonlinear vibration with the broadband frequency to the water tank. The strong vibration of the IV earthquake lasted a long time, while the SF earthquake had strong instantaneous vertical displacement and short duration. Both the ground motions in the longitudinal (*X* direction) and vertical (*Y* direction) directions were considered, instead of the condition in which only longitudinal displacement was applied in previous studies [23,24]. By the way, the location of the SF earthquake is close to the water tank in Haroun. Therefore, the water motion under these different excitations might perform differently. Each of the ground motions was scaled to the same peak ground acceleration (PGA) of 0.5 g so that they represented the same earthquake intensity. The information of the two scaled earthquake events is listed in Table 2, and the scaled ground motions are shown in Figure 6.

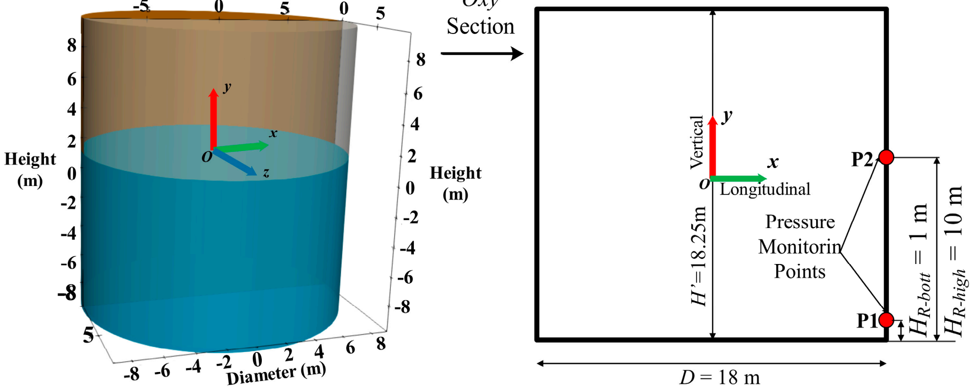

Figure 5. The geometry of the water storage tank.

Table 1. Grid dependence of the free surface elevation at the right side wall under the Imperial Valley (IV) earthquake.

Mesh	Description	Maximum Size (x × y)	Calculation Time (s)	Averaged Free Surface Peaks at Right Side Wall (x = 9 m)	Relative Difference
1	Fine	0.075 × 0.025	3391	0.1839 m	-
2	Medium (used)	0.15 × 0.05	464	0.1746 m	5%
3	Coarse	0.3 × 0.1	88	0.1580 m	14%

Table 2. Information of two strong ground motions. PGA: peak ground acceleration, SF: San Fernando.

Earthquake Event	Scaled PGA (g)	Scale Factor	Scaled PGD* (m)	Strong Motion Duration (s)
IV	Longitudinal: 0.5 Vertical: 0.317	1.78	Longitudinal: 0.154 Vertical: 0.048	30
SF	Longitudinal: 0.5 Vertical: 0.282	0.41	Longitudinal: 0.160 Vertical: 0.120	18

PGD*: peak ground displacement.

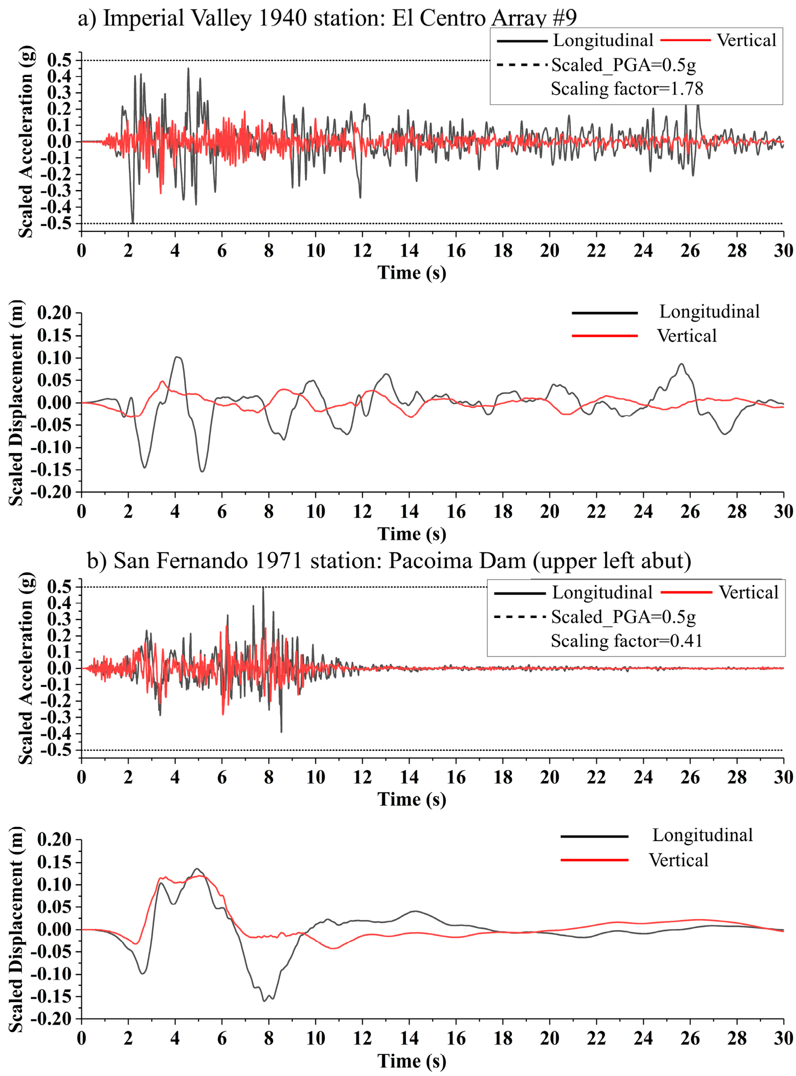

Figure 6. Acceleration and displacement of two selected earthquakes, (**a**) the scaled acceleration and the displacement of the Imperial Valley 1940 earthquake, (**b**) the scaled acceleration and the displacement of the San Fernando 1971 earthquake.

3. Results and Discussion

3.1. Comparison of Water Motion between Two-Dimensional and Three-Dimensional Results

In order to make the calculation process economical, the *Oxy* section was extracted to study the water sloshing in the tank under seismic excitation. However, in case the 2D simulation can be used instead of the real 3D status, the comparison of water motion between the 2D and 3D problems was conducted. A similar trend can be seen in Figure 7. The free surface at the *Oxy* ($Z = 0$) section in the 3D simulation coincided with the 2D result. Meanwhile, it can be seen that the free surface elevation decreased along the *Z* direction from 0 to ±9 m (*Oyz* section of the tank) in the 3D model, which is different from the previous research in a cube tank [10]. They showed a similar sloshing response in the *Z* direction. This is because we used a cylindrical tank, and the side wall of the tank was a curved surface. Further investigation of the two models is supplied in Figure 8.

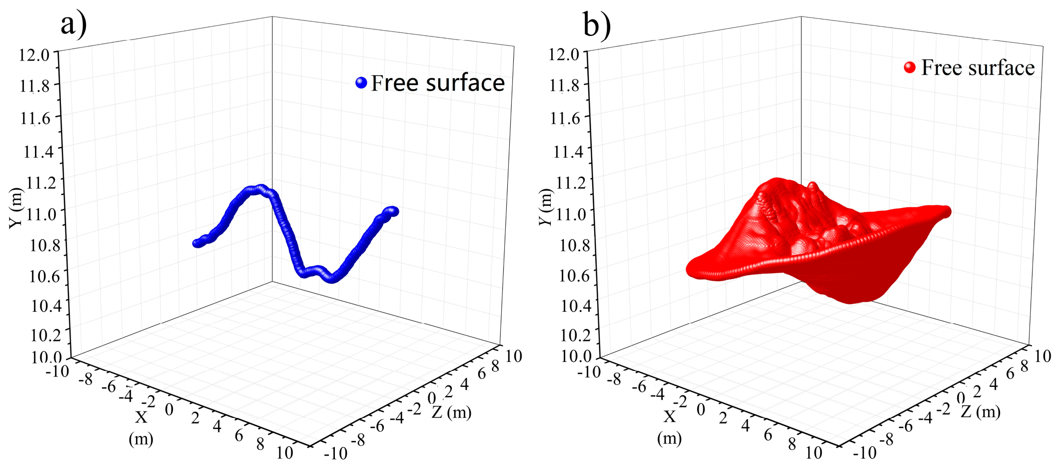

Figure 7. Free surface shape of the sloshing in the water tank under the IV earthquake, (**a**) 2D case, $t = 10.25$ s, (**b**) 3D case, $t = 10.25$ s.

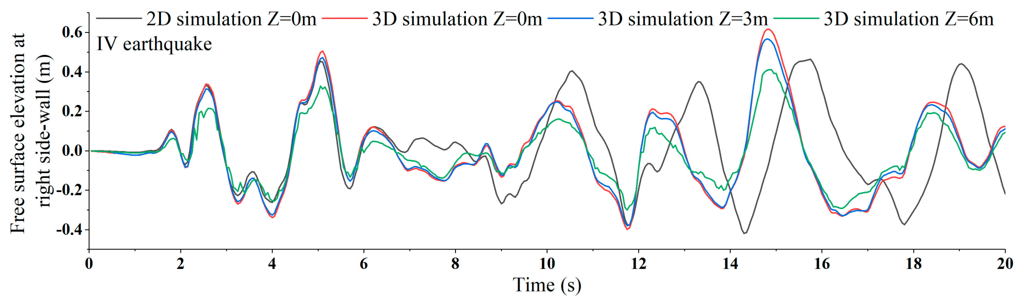

Figure 8. Free surface elevations at the right side wall.

The maximum free surface elevation appeared at the *Oxy* section of the tank, as seen in Figure 8. In this study, the free surface on the *Oxy* section was extracted to show the water sloshing in the tank under seismic excitation. This result usually indicated the most dangerous section of the tank. Therefore, in order to save time and calculation costs, the water movement in the most dangerous section was calculated here mainly based on the 2D simulation. The free surface shape and the time history of elevation between the 2D and 3D simulation are further shown in Figures 8 and 9. They indicated that the 2D results were acceptable. Therefore, the motion response of water and the conclusions drawn from it should be meaningful.

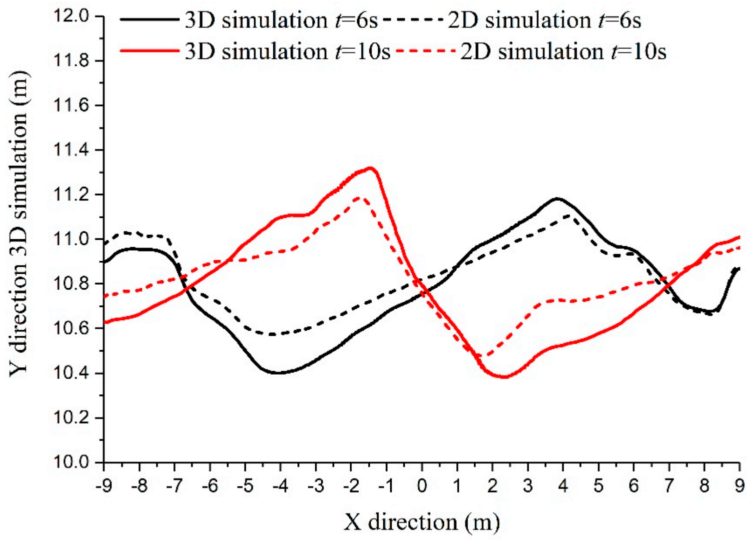

Figure 9. Free surface response at selected moments.

3.2. Free Surface Motion in the High Filling Depth Water Tank under Seismic Excitation

From Figure 6, the largest longitudinal and vertical PGDs appeared in the first 10 s of the ground motions. During this stage, the shapes of the free surface at the 2 s, 4 s, 6 s, 8 s, and 10 s and the Fast Fourier Transfer (FFT) amplitudes of two ground motions are shown in Figure 10. The results showed that the response of the water reached the maximum displacement of the tank. Although the maximum instantaneous displacement of the SF earthquake was larger (see Table 1), the free liquid motion caused by it was not significantly more violent than that of the IV earthquake. The maximum free surface elevations of the two earthquakes reached 11.20 m and 11.19 m, respectively. The ratio of the free surface elevation to the original water level was only 3.7% for the IV earthquake and 3.6% for the SF earthquake. There is no significant difference here.

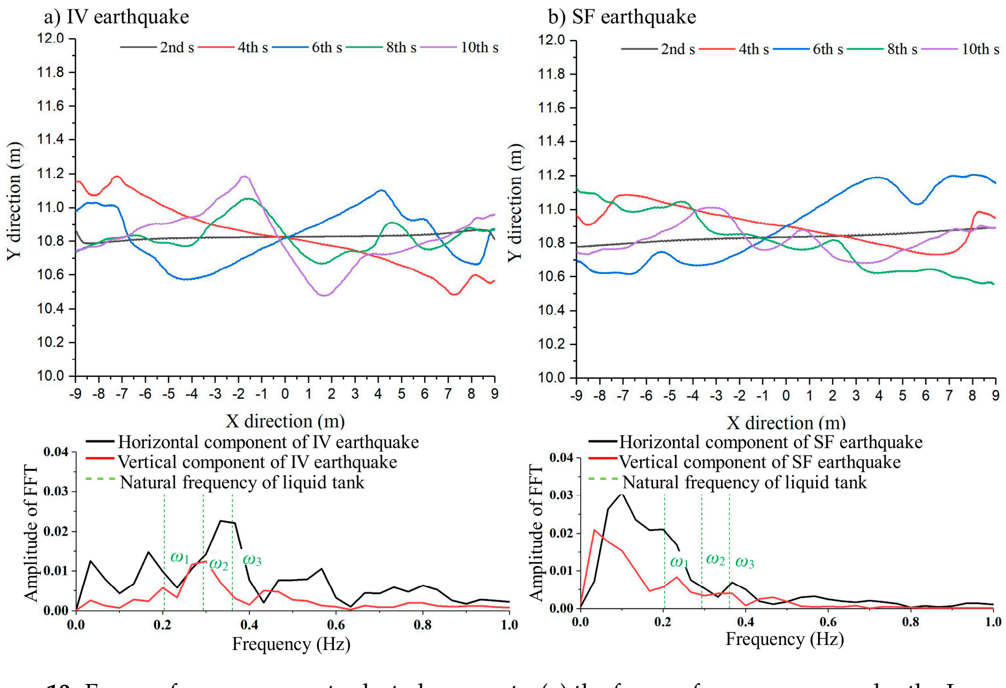

Figure 10. Free surface response at selected moments, (**a**) the free surface response under the Imperial Valley 1940 earthquake, (**b**) the free surface response under the San Fernando 1971 earthquake.

The free surface shapes are shown in Figure 10, indicating that the location of the largest node of water vibration is different. The nodes in IV are located around 1/3*D* and 2/3*D*, and the nodes in SF are located at the side wall. They corresponded to the first and third modes sloshing in the water tank, respectively [39]. Based on the Fast Fourier Transfer (FFT), the seismic excitations were transferred to the frequency domain, and the first three natural frequencies ($\omega_{i,}$ i = 1, 2, 3) were marked. The results showed that the primary frequencies of SF and IV were close to ω_1 and ω_3, respectively. Therefore, the corresponding sloshing modes were excited. On the other hand, the odd resonance modes of sloshing are (n = 1, 3, ...) usually activated by the anti-symmetric motion (sway in the horizontal direction) of the container, and even the resonance modes (n = 2, 4, ...) corresponded to the symmetric motion (heavy in the vertical direction). The FFT results in Figure 10 indicated that the resonance sloshing is more likely to occur under the IV earthquake.

The envelopes of the maximum free surface revealed that the effects of water on the tank walls were similar (Figure 11), although the excitations of the ground motion were irregular and asymmetric. Meanwhile, the maximum free surface elevation appeared near the side wall, and the minimum point was located at the center of the still water level. The high-water level at the tank wall of the water tank is also usually the cause of the destruction and overturning of the tank. The maximum rate of free surface elevation was 6.58% for the IV earthquake and 8.20% for the SF earthquake. These results mean that earthquakes with large instantaneous displacements, such as the SF earthquake, may lead to more dangerous situations. This was inconsistent with the conclusion reflected in the response of the water motion during the first 10 s when a large ground displacement occurred. Therefore, the time history of the free surface elevation at the right side wall is shown in Figure 12 to help understand the above phenomenon. Figure 12 shows that the sloshing was not fully excited in the early stage of the earthquake. The maximum free surface response did not appear at the stage when the maximum ground displacement occurred, and the sloshing phenomenon continued and kept growing, despite the large ground displacement having passed. The elevation decreased after 10 s in the SF earthquake event. The water kept sloshing stably in the IV earthquake event until a new seismic pulse peak appeared, and the elevation increased again. The above results indicated that the sloshing excited by the seismic motion was hysteretic compared with the ground motion. Therefore, the water storage tank still faced the threat of collapse, although the violent ground motion passed.

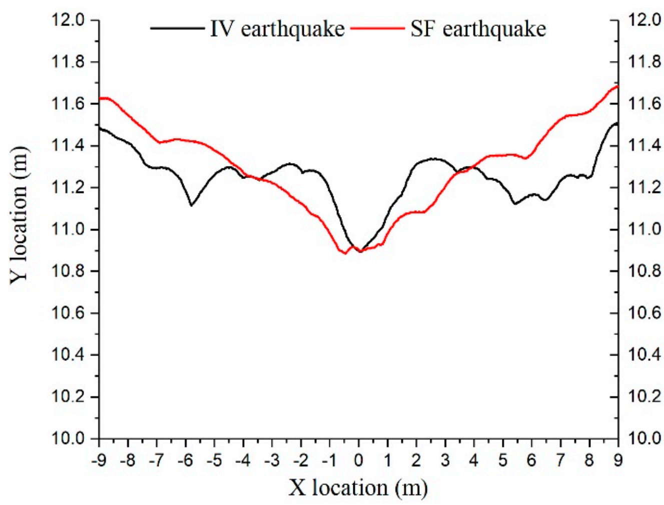

Figure 11. The maximum free surface envelope under two different ground motions.

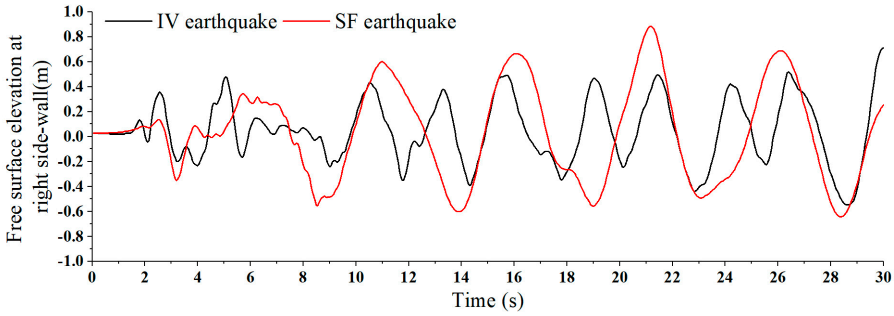

Figure 12. Free surface elevations at right side wall.

3.3. Seismic Design of the Water Storage Tank and the Anti-Sloshing Ability of the Damping Baffle

Even a short-term seismic pulse will cause continuous sloshing in the water storage tank and bring a sloshing load, which delayed more than the ground motion. For the safety design of the water tank in earthquake-prone areas, a well-studied vertical damping baffle (see Figure 13) was used to test its suppression on sloshing, such as [15,20,40,41]. The height of the baffle $a = 2/3d$. The mesh around the baffle was refined. Figure 14 gives the free surface elevations at the right side wall in the cases of tanks with and without the damping baffle. The results showed that the vertical damping baffle had a better effect on the free surface elevations at the side wall, under the SF earthquake.

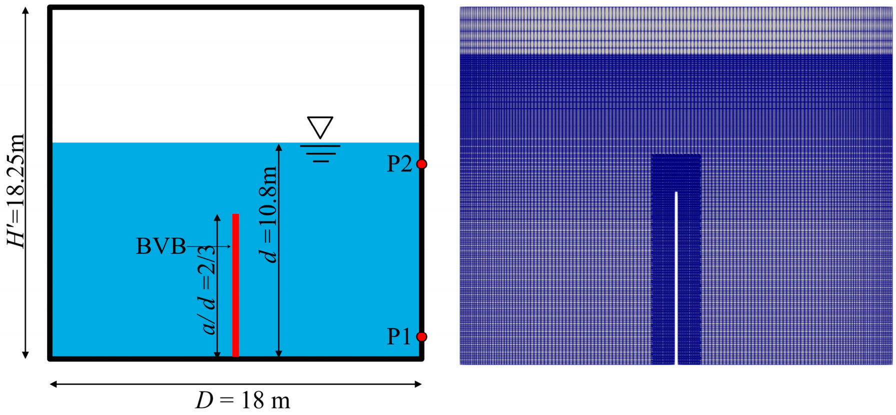

Figure 13. Location of the damping baffle in the water tank and mesh geometry.

On the other hand, the sloshing pressure on the two measuring points with and without the damping baffle was compared. The two measuring points were located near the bottom and the free surface of the water tank, which were 1 m and 10 m away from the bottom, respectively. Then, the pressure variation at these two points is shown in Figure 15, and the sloshing pressures were normalized by $p/\rho gh$-1 to express the fluctuation of sloshing pressure. Here, the ρgh was the hydrostatic pressure at the selected points. The results showed that the pressure variation ratio near the water surface was larger than that in the bottom area. The damping baffle had a significant suppression effect on the sloshing pressure near the free liquid surface, but this only occurred after the violent ground motion passed. The pressure and free surface elevation had similar trends due to the seismic excitation.

With the damping baffle, the maximum response of the sloshing surface and the pressure at the selected points P1 and P2 were suppressed by 16.8%, 5.0%, and 3.5% under the IV earthquake and 37.2%, 0.5%, and 4.2% for the SF earthquake. Then, the conclusion can be drawn that the suppression of sloshing pressure by the vertical damping baffle was limited under the nonlinear seismic excitation, although it can suppress the water motion well. That is probably because the vertical baffle suppressed the violent sloshing through its function of resonant frequency tuning. Since the nonlinear seismic excitation and the structural differences in size and the filling level may cause the different pressure response and the water motion, the results of the baffle configuration in the previous sloshing study cannot be applied directly to the seismic design of the tank. Therefore, analysis of the water motion and pressure within a water storage tank under an earthquake load is still needed.

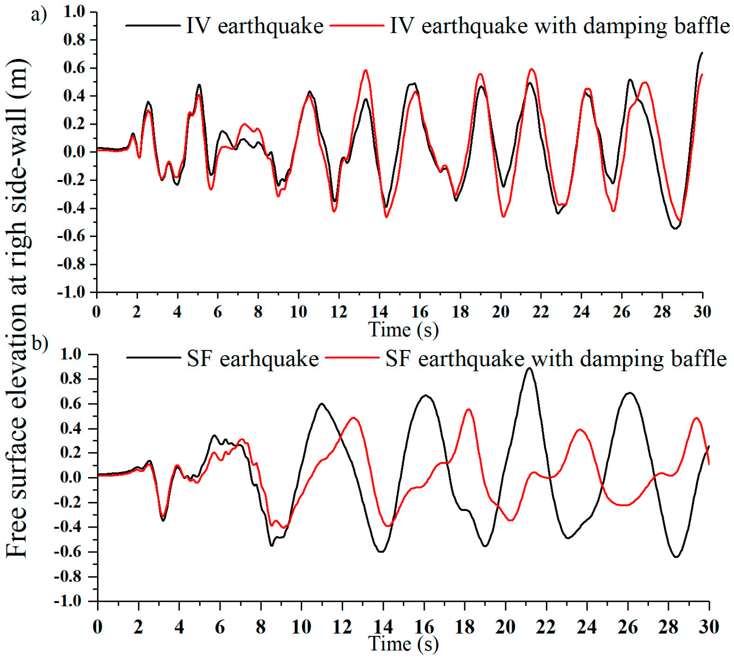

Figure 14. The suppression effect of the vertical damping baffle on sloshing water, (**a**) the free surface elevation under the Imperial Valley 1940 earthquake, (**b**) the free surface elevation under the San Fernando 1971 earthquake.

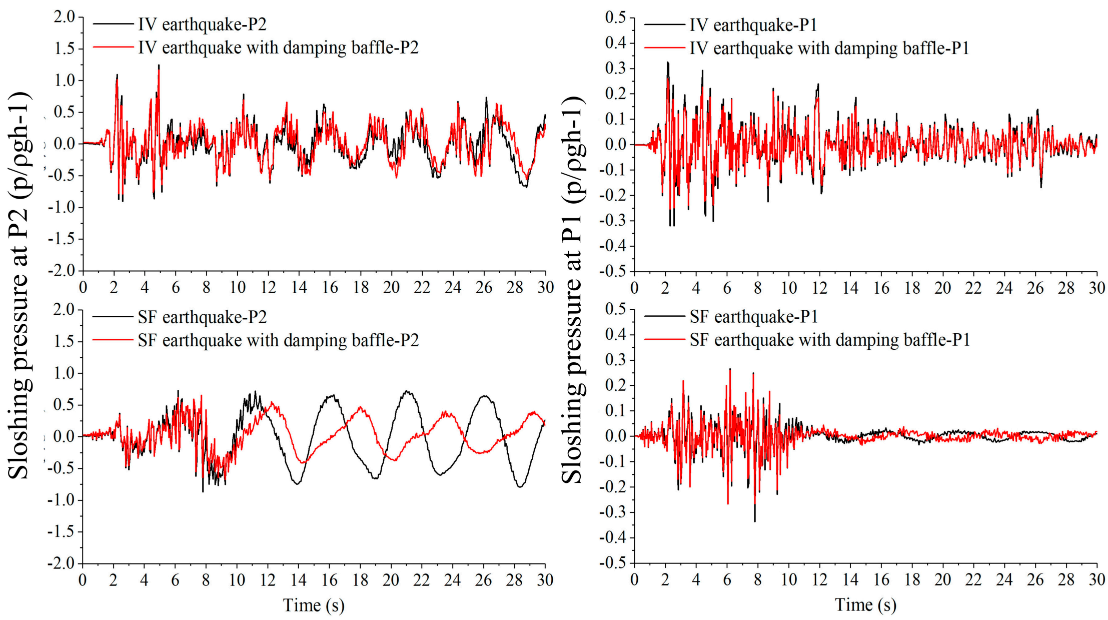

Figure 15. The fluctuation of sloshing pressure at selected points.

4. Conclusions

The water motion in a real-scale water storage tank under two well-studied ground motions were investigated based on the OpenFOAM in this study. The experimental tests were conducted for validation of the present numerical model. The larger tank size, the high filling level, and the nonlinear seismic excitation were considered in this research. Other than the previous studies on sloshing in a rectangular water tank, the results under the current conditions were slightly different in terms of baffle configuration design, pressure response, and water sloshing.

(1) A comparison between 2D and 3D results of the water sloshing in a cylindrical tank was conducted. The 2D analysis could be used to predict the water sloshing response in a cylindrical tank. The *Oxy* section gave the maximum free surface elevation of the sloshing, and the most dangerous condition can be covered.

(2) Due to the huge size of the water tank and the large mass of the filled water, the free surface motion was small, even under the strong ground motion. The maximum free surface elevation did not exceed 10%.

(3) Similar to the response under the harmonic excitation, the free surface motion still satisfied the sloshing modal characteristic under seismic excitation. The maximum free surface elevation appeared at the side wall, and there were two nodes when the seismic frequency was close to the third-order natural frequency of the water tank.

(4) In addition, the water motion was hysteretic compared with the ground motion. The maximum free surface elevation appeared after the seismic wave passed instead of the seismic wave was passing. Meanwhile, the pressure response was different, which kept decreasing after the strong seismic wave passed.

(5) The effect of the well-used vertical damping baffle on the suppression of sloshing pressure was limited when the strong ground motion was passing. Further study about the seismic design of the water storage tank is still needed.

Author Contributions: Writing—original draft, H.J.; Writing—review and editing, R.S. and Y.L. All authors have read and agreed to the published version of the manuscript.

Funding: This research was funded by the Natural Science Foundation of Zhejiang, grant number LQ19E090005, the Natural Science Foundation of Ningbo, grant number 2019A610164 and National Natural Science Foundation of China, grant number 51605431.

Conflicts of Interest: The authors declare no conflict of interest.

References

1. Soroushnia, S.; Tafreshi, S.T.; Omidinasab, F.; Beheshtian, N.; Soroushnia, S. Seismic performance of RC elevated water tanks with frame staging and exhibition damage pattern. *Procedia Eng.* **2011**, *14*, 3076–3087. [CrossRef]
2. Korkmaz, K.A.; Sari, A.; Carhoglu, A.I. Seismic risk assessment of storage tanks in Turkish industrial facilities. *J. Loss Prev. Process Ind.* **2011**, *24*, 314–320. [CrossRef]
3. Vakilaadsarabi, A.; Miyajima, M.; Murata, K. Study of the Sloshing of Water Reservoirs and Tanks due to Long Period and Long Duration Seismic Motions. In Proceedings of the 15th World Conference on Earthquake Engineering, Lisbon, Portugal, 24–28 September 2012; pp. 1–10.
4. Zama, S.; Nishi, H.; Yamada, M.; Hatayama, K. Damage of Oil Storage Tanks Caused by Liquid Sloshing in the 2003 Tokachi Oki Earthquake and Revision of Design Spectra in the Long-Period Range. In Proceedings of the 14th World Conference on Earthquake Engineering, Beijing, China, 12–17 October 2008; pp. 1–8.
5. Faltinsen, O.M.; Timokha, A.N. *Sloshing*; Cambridge University Press: Cambridge, UK, 2009.
6. Frandsen, J.B. Sloshing motions in excited tanks. *J. Comput. Phys.* **2004**, *196*, 53–87. [CrossRef]
7. Faltinsen, O.M.; Timokha, A.N. An adaptive multimodal approach to nonlinear sloshing in a rectangular tank. *J. Fluid Mech.* **2001**, *432*, 167–200. [CrossRef]
8. Virella, J.C.; Prato, C.A.; Godoy, L.A. Linear and nonlinear 2D finite element analysis of sloshing modes and pressures in rectangular tanks subject to horizontal harmonic motions. *J. Sound Vib.* **2008**, *312*, 442–460. [CrossRef]
9. Gavrilyuk, I.; Lukovsky, I.; Trotsenko, Y.; Timokha, A. Sloshing in a vertical circular cylindrical tank with an annular baffle. Part 1. Linear fundamental solutions. *J. Eng. Math.* **2006**, *54*, 71–88. [CrossRef]
10. Chen, Y.; Xue, M.A. Numerical simulation of liquid sloshing with different filling levels using OpenFOAM and experimental validation. *Water* **2018**, *10*, 1752. [CrossRef]

11. Akyldz, H.; Erdem Ünal, N.; Aksoy, H. An experimental investigation of the effects of the ring baffles on liquid sloshing in a rigid cylindrical tank. *Ocean Eng.* **2013**, *59*, 190–197. [CrossRef]
12. Faltinsen, O.M.; Timokha, A.N. Analytically approximate natural sloshing modes for a spherical tank shape. *J. Fluid Mech.* **2012**, *703*, 391–401. [CrossRef]
13. Isaacson, M.; Premasiri, S. Hydrodynamic damping due to baffles in a rectangular tank. *Can. J. Civ. Eng.* **2001**, *28*, 608–616. [CrossRef]
14. Biswal, K.C.; Bhattacharyya, S.K.; Sinha, P.K. Non-linear sloshing in partially liquid filled containers with baffles. *Int. J. Numer. Methods Eng.* **2006**, *68*, 317–337. [CrossRef]
15. Faltinsen, O.M.; Firoozkoohi, R.; Timokha, A.N. Analytical modeling of liquid sloshing in a two-dimensional rectangular tank with a slat screen. *J. Eng. Math.* **2011**, *70*, 93–109. [CrossRef]
16. Lee, D.H.; Kim, M.H.; Kwon, S.H.; Kim, J.W.; Lee, Y.B. A parametric sensitivity study on LNG tank sloshing loads by numerical simulations. *Ocean Eng.* **2007**, *34*, 3–9. [CrossRef]
17. Jin, H.; Liu, Y.; Song, R.; Liu, Y. Analytical Study on the Effect of a Horizontal Perforated Plate on Sloshing Motion in a Rectangular Tank. *J. Offshore Mech. Arct. Eng.* **2020**, *142*. [CrossRef]
18. Jin, H.; Liu, Y.; Li, H.; Fu, Q. Numerical analysis of the flow field in a sloshing tank with a horizontal perforated plate. *J. Ocean Univ. China* **2017**, *16*, 575–584. [CrossRef]
19. Jin, H.; Liu, Y.; Li, H.J. Experimental study on sloshing in a tank with an inner horizontal perforated plate. *Ocean Eng.* **2014**, *82*, 75–84. [CrossRef]
20. Xue, M.A.; Zheng, J.; Lin, P.; Yuan, X. Experimental study on vertical baffles of different configurations in suppressing sloshing pressure. *Ocean Eng.* **2017**, *136*, 178–189. [CrossRef]
21. Chen, W.; Haroun, M.A.; Liu, F. Large amplitude liquid sloshing in seismically excited tanks. *Earthq. Eng. Struct. Dyn.* **1996**, *25*, 653–669. [CrossRef]
22. Huerta-Lopez, C.I.; Shin, Y.; Powers, E.J.; Roesset, J.M. Time-frequency analysis of earthquake records. In Proceedings of the 12th World Conference on Earthquake Engineering, Auckland, New Zealand, 30 January–4 February 2000; pp. 1–8.
23. Chen, Y.-H.; Hwang, W.-S.; Ko, C.-H. Sloshing behaviours of rectangular and cylindrical liquid tanks subjected to harmonic and seismic excitations. *Earthq. Eng. Struct. Dyn.* **2007**, *36*, 1701–1717. [CrossRef]
24. Xue, M.; Chen, Y.; Yuan, X.; Dou, P. A Study on Effects of the Baffles in Reducing Sloshing in a Container under Earthquake Excitation. In Proceedings of the Twenty-ninth (2019) International Ocean and Polar Engineering Conference, Hawaii, HI, USA, 16–21 June 2019; pp. 3393–3397.
25. Faltinsen, O.M.; Timokha, A.N. Asymptotic modal approximation of nonlinear resonant sloshing in a rectangular tank with small fluid depth. *J. Fluid Mech.* **2002**, *470*, 319–357. [CrossRef]
26. Ockendon, H.; Ockendon, J.R.; Johnson, A.D. Resonant sloshing in shallow water. *J. Fluid Mech.* **1986**, *167*, 465–479. [CrossRef]
27. Bouscasse, B.; Antuono, M.; Colagrossi, A.; Lugni, C. Numerical and experimental investigation of nonlinear shallow water sloshing. *Int. J. Nonlinear Sci. Numer. Simul.* **2013**, *14*, 123–138. [CrossRef]
28. Waterhouse, D.D. Resonant Sloshing Near a Critical Depth. *J. Fluid Mech.* **1994**, *281*, 313–318. [CrossRef]
29. Rognebakke, O.F.; Faltinsen, O.M. Sloshing induced impact with air cavity in rectangular tank with a high filling ratio. In Proceedings of the 20th International Workshop on Water Waves and Floating Bodies, Spitsbergen, Norway, 29 May–1 June 2005.
30. Jasak, H.; Jemcov, A.; Tukovic, Z. OpenFOAM: A C++ library for complex physics simulations. In Proceedings of the International Workshop on Coupled Methods in Numerical Dynamics, Dubrovnik, Croatia, 19–21 September 2007; pp. 1–20.
31. Liu, D.; Tang, W.; Wang, J.; Xue, H.; Wang, K. Comparison of laminar model, RANS, LES and VLES for simulation of liquid sloshing. *Appl. Ocean Res.* **2016**, *59*, 638–649. [CrossRef]
32. Faltinsen, O.M. A numerical nonlinear method of sloshing in tanks with two-dimensional flow. *J. Ship Res.* **1978**, *22*, 193–202.
33. Faltinsen, O.M.; Firoozkoohi, R.; Timokha, A.N. Steady-state liquid sloshing in a rectangular tank with a slat-type screen in the middle: Quasilinear modal analysis and experiments. *Phys. Fluids* **2011**, *23*. [CrossRef]
34. Haroun, M.A. Vibration studies and tests of liquid storage tanks. *Earthq. Eng. Struct. Dyn.* **1983**, *11*, 179–206. [CrossRef]

35. Jones, L.M.; Hauksson, E. Evaluation of Earthquake Potential in Southern California. In Proceedings of the Future directions in evaluating earthquake hazards of southern California, Los Angeles, CA, USA, 12–13 November 1985; pp. 63–72.
36. Goudarzi, M.A.; Sabbagh-Yazdi, S.R. Analytical and experimental evaluation on the effectiveness of upper mounted baffles with respect to commonly used baffles. *Ocean Eng.* **2012**, *42*, 205–217. [CrossRef]
37. Faltinsen, O.M. Sloshing. *Adv. Mech.* **2017**, *47*, 1–24. [CrossRef]
38. Ancheta, T.D.; Darragh, R.B.; Stewart, J.P.; Seyhan, E.; Silva, W.J.; Chiou, B.S.J.; Wooddell, K.E.; Graves, R.W.; Kottke, A.R.; Boore, D.M.; et al. NGA-West2 database. *Earthq. Spectra* **2014**, *30*, 989–1005. [CrossRef]
39. Sanapala, V.S.; Rajkumar, M.; Velusamy, K.; Patnaik, B.S.V. Numerical simulation of parametric liquid sloshing in a horizontally baffled rectangular container. *J. Fluids Struct.* **2018**, *76*, 229–250. [CrossRef]
40. Demirel, E.; Aral, M. Liquid Sloshing Damping in an Accelerated Tank Using a Novel Slot-Baffle Design. *Water* **2018**, *10*, 1565. [CrossRef]
41. Dinçer, A.E. Investigation of the sloshing behavior due to seismic excitations considering two-way coupling of the fluid and the structure. *Water* **2019**, *11*, 2664. [CrossRef]